///VSP/// Advanced Robotics 22 (2008) 1267–1285
ADVANCED ROBOTICS
www.brill.nl/ar

Full paper

A Tire Stiffness Backstepping Observer Dedicated to All-Terrain Vehicle Rollover Prevention

Nicolas Bouton [a,*], **Roland Lenain** [a], **Benoit Thuilot** [b] **and Philippe Martinet** [b,c]

[a] Cemagref, 24 avenue des Landais, BP 50085, 63172 Aubière Cedex, France
[b] LASMEA, 24 avenue des Landais, 63177 Aubière Cedex, France
[c] ISRC, Sungkyunkwan University, Suwon, South Korea

Received 15 January 2008; accepted 28 March 2008

Abstract

Most active devices focused on vehicle stability concern on-road cars and cannot be applied satisfactorily in an off-road context, since the variability and the non-linearities of tire/ground contact are often neglected. In previous work, a rollover indicator devoted to light all-terrain vehicles accounting for these phenomena has been proposed. It is based on the prediction of the lateral load transfer. However, such an indicator requires the on-line knowledge of the tire cornering stiffness. Therefore, in this paper, an adapted backstepping observer, making use only of yaw rate measurement, is designed to estimate tire cornering stiffness and to account for its non-linearity. The capabilities of such an observer are demonstrated and discussed through both advanced simulations and actual experiments.

Keywords

Backstepping observer, tire cornering stiffness, all-terrain vehicles, rollover prevention

1. Introduction

Light manned and unmanned all-terrain vehicles (ATVs), such as quad bikes or exploration robots, are designed to provide good driveability. However, their associated geometric characteristics (small wheelbase, track width and weight) may lead to unsafe vehicle behavior and may increase their propensity to roll over. This is a serious concern, in view of their growing popularity. For instance, in the USA, the Consumer Product Safety Commission [1] reported 7188 fatal quad bike accidents between 1982 and 2003, and has collected a list of 136 700 injuries resulting from the use of manned ATVs for 2005 alone. The same year, 50 quad bike ac-

* To whom correspondence should be addressed. E-mail: nicolas.bouton@cemagref.fr

 DOI:10.1163/156855308X344828

cidents were listed by a French insurance company [2] in the agricultural sector alone. As a result, the development of on-board devices improving off-road vehicle stability constitutes an important issue, since it can both reduce the number of manned ATV injuries and guarantee the safety of mobile robots where classical motion control laws do not account for rollover risks in a natural environment context. Developments proposed in this paper address both manually or automatically controlled vehicles.

Several solutions have already been proposed for on-road vehicles in the robotics community: steering and braking control [3, 4] or electronic stability program systems [5] are some examples. However, since car-like vehicles are supposed to move on high grip ground, such devices consider only pseudo-sliding phenomena with constant tire cornering stiffness. In contrast, field robots are supposed to move on natural ground with highly variable contact conditions. Therefore, stability devices suitable for cars cannot be directly adapted to ATVs. The aim of our current research, therefore, focuses on the development of ATV rollover avoidance devices.

Since such security devices are intended to be activated only in hazardous situations, some rollover indicators have to be developed. In the literature, two kinds of metrics have been developed to assess rollover risk. The first category consists of static stability indicators such as the static stability factor [6]. Such indicators do not require numerous or expensive sensors, since they are only based on the vehicle's geometrical characteristics [7]. However, they do not integrate sliding phenomena and are not able to represent dynamic rollover situations. The second category, composed of dynamic metrics, appears to be more relevant to the anticipation of ATV rollover situations. Nevertheless, some of these indicators — especially zero moment point (ZMP) [8, 9] or lateral acceleration approaches [3] — cannot be directly used in an ATV context, since they require an expensive sensor configuration relative to the cost of the ATV (e.g., dynamometric wheel sensors for ZMP computation) or rely on thresholds particularly difficult to tune on slippery ground (critical thresholds on lateral acceleration).

Our proposed device, therefore, relies on a dynamic rollover risk indicator evaluated from the lateral load transfer (LLT) [10]. This indicator is derived from the estimation of wheel normal forces based on a low-cost sensor set and the LLT critical threshold is quite easy to tune, since lift-off of the left or right wheels of the vehicle corresponds to a unitary LLT value.

Since ATVs move on natural ground, the non-linear behavior of the tire must be taken into account when estimating the normal forces of the vehicle. Therefore, the tire/ground grip properties have to be estimated on-line since they affect the rollover propensity (as highlighted in Ref. [11]). A preliminary solution, detailed in Ref. [10], proposes a network of several ground classes selected on-line with respect to the measured ATV yaw rate. However, the main drawbacks of this approach are, on the one hand, the required off-line calibration of the ground classes and, on the other hand, the inaccuracy of the algorithm when grip conditions are far from any ground class. To overcome these negative aspects, an alternative approach, taking advantage of observer theory, is considered here. If observers have already been proposed [12–14] to obtain an estimation of tire cornering stiffness, these approaches need expensive sensors (high-accuracy GPS and an inertial navigation system) so that key vehicle state variables are available. Such complex perception systems can be on-board on road vehicles, but are not consistent with the light vehicles considered in this paper. This issue is, therefore, addressed with a more realistic sensor configuration composed of a gyrometer, a steering angle sensor and a Doppler radar.

The paper is organized as follows. First, a simple dynamic model combined with a linear tire model is defined. Then, a preliminary linear yaw rate observer assuming constant tire cornering stiffness is developed to demonstrate the impossibility of accurately estimating key vehicle state variables when the tire/ground forces are non-linear. A new observer based on a backstepping approach was, therefore, designed to estimate the current yaw rate of the vehicle, thanks to the adaptation of a virtual tire cornering stiffness accounting for tire/ground contact non-linearities and variability. Finally, the relevance of the virtual tire cornering stiffness thus obtained is discussed with reference to both advanced simulations and on-line computation of the LLT in actual experiments.

2. Vehicle Modeling

2.1. Dynamic Bicycle Model

We are interested in accounting for sliding in vehicle lateral dynamics. The vehicle model is therefore based on an Ackermann model [15] extended with sliding parameters, as described in Ref. [16] and shown in Fig. 1. Notations used in this paper are: G is the vehicle center of gravity, L is the vehicle wheelbase, a and b are the front and rear half-wheelbases, respectively, δ is the steering angle, v is the linear velocity at the center of the rear axle, u is the linear velocity at the center of gravity, ψ is the vehicle yaw angle, β is the global sideslip angle of the vehicle, α_{r} and

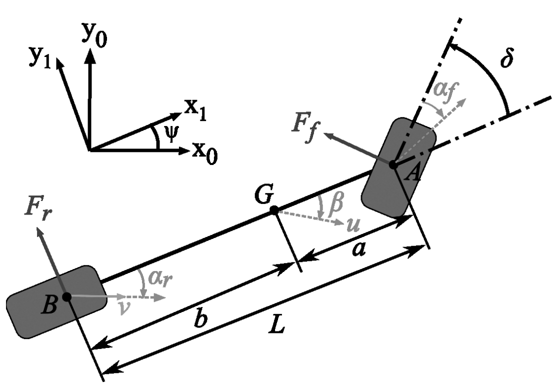

Figure 1. Dynamic bicyle model with sliding parameters.

α_f are the rear and front sideslip angles, respectively, and F_f and F_r are the lateral forces generated on the front and rear tires, respectively.

2.2. Tire Forces Model

Since sliding parameters and tire/ground forces have been added into the yaw representation of the vehicle, a tire/ground contact model has to be chosen. As described in Ref. [17], several models can be used to describe sliding phenomena (such as the Pacejka model [18]). However, such models require numerous and varying parameters, hardly accessible in real-time. As a consequence, for on-line applications at the considered high velocities, the simpler linear model (1) is considered here:

$$\begin{cases} F_\mathrm{f} = C_\mathrm{f}(\cdot)\alpha_\mathrm{f} \\ F_\mathrm{r} = C_\mathrm{r}(\cdot)\alpha_\mathrm{r}, \end{cases} \tag{1}$$

where $C_\mathrm{f}(\cdot)$ and $C_\mathrm{r}(\cdot)$ are the front and rear tire cornering stiffnesses, respectively, greatly dependent on several aspects such as tire normal forces and grip condition variations. As discussed in Section 3.3, in order to take into account the non-linear behavior of the tire, these tire cornering stiffnesses will be estimated on-line.

2.3. Dynamic Equations

Relying on both the linear tire model and the bicycle model representation shown in Fig. 1, motion equations can be derived by using the fundamental principle of the dynamic, as shown in Ref. [15, 19]. When longitudinal forces are neglected (which is realistic here since only the lateral vehicle dynamic is studied and described by yaw rate and sideslip angles), motion equations are given by:

$$\begin{cases} \ddot{\psi} = \dfrac{1}{I_z}(-aC_\mathrm{f}\alpha_\mathrm{f}\cos(\delta) + bC_\mathrm{r}\alpha_\mathrm{r}) \\ \dot{\beta} = -\dfrac{1}{um}(C_\mathrm{f}\alpha_\mathrm{f}\cos(\beta-\delta) + C_\mathrm{r}\alpha_\mathrm{r}\cos(\beta)) - \dot{\psi} \\ \alpha_\mathrm{r} = a\tan\left(\beta - \dfrac{b\dot{\psi}}{u}\right) \\ \alpha_\mathrm{f} = a\tan\left(\beta + \dfrac{a\dot{\psi}}{u}\right) - \delta \\ u = \dfrac{v\cos(\alpha_\mathrm{r})}{\cos(\beta)}, \end{cases} \tag{2}$$

where I_z and m are the yaw inertial momentum and the mass of the vehicle, respectively.

3. Observer Design

In this paper three measurements are used to estimate both the vehicle yaw rate and the tire cornering stiffness: the steering angle (available from an angle sensor), the yaw rate (from a low-cost gyrometer) and the rear axle linear velocity (from a Doppler radar). They are realistic sensors with respect to the cost and small size of these ATVs.

The two observers presented in this paper were developed assuming that the velocity at the vehicle's center of gravity is equal to that of the vehicle's rear axle (i.e., $\|\vec{u}\| \approx \|\vec{v}\|$ in Fig. 1). This hypothesis is realistic as long as both the global sideslip angle and the rear sideslip angle are relatively small (see (2)), which is generically true for ATVs when rollover events are avoided.

3.1. Linear Observer (LO)

This first observer was developed on the assumption of constant tire cornering stiffnesses. This will show the impact of such a restrictive hypothesis on the yaw rate observation error with respect to actual grip conditions.

3.1.1. State Space Equations

Assuming that sideslip angles are quite small (less than 10° in practice), the equations (2) can be linearized. This leads to the following state space system:

$$\dot{X} = AX + B\delta, \tag{3}$$

with $X = (\dot{\psi} \quad \beta)^{\mathrm{T}}$, $A = \begin{bmatrix} a_{11} & a_{12} \\ a_{21} & a_{22} \end{bmatrix}$ and $B = \begin{bmatrix} b_1 \\ b_2 \end{bmatrix}$ and $a_{11} = (-a^2C_{\mathrm{f}} - b^2C_{\mathrm{r}})/(vI_z)$, $a_{12} = (-aC_{\mathrm{f}} + bC_{\mathrm{r}})/I_z, a_{21} = -((aC_{\mathrm{f}} - bC_{\mathrm{r}}))/(mv^2) - 1, a_{22} = -(C_{\mathrm{r}} + C_{\mathrm{f}})/(mv), b_1 = aC_{\mathrm{f}}/I_{\mathrm{z}}$ and $b_2 = C_{\mathrm{f}}/(mv)$. Relying on the available measurements, the observation equation is:

$$Y = CX = [\,1 \;\; 0\,]\begin{bmatrix} \dot{\psi} \\ \beta \end{bmatrix}. \tag{4}$$

3.1.2. Observability

The Kalman observability matrix O can easily be computed:

$$O = \begin{bmatrix} C \\ CA \end{bmatrix} = \begin{bmatrix} 1 & 0 \\ a_{11} & a_{12} \end{bmatrix} = \begin{bmatrix} 1 & 0 \\ \dfrac{-a^2C_{\mathrm{f}} - b^2C_{\mathrm{r}}}{vI_z} & \dfrac{-aC_{\mathrm{f}} + bC_{\mathrm{r}}}{I_z} \end{bmatrix}. \tag{5}$$

According to (5), matrix O is invertible if $a_{12} \neq 0$, which is true as soon as $aC_{\mathrm{f}} \neq bC_{\mathrm{r}}$ (generally satisfied since $C_{\mathrm{r}} > C_{\mathrm{f}}$ and $b > a$ on most ATVs and for standard grip conditions) and of course if $v \neq 0$. Therefore, the system is observable.

3.1.3. Linear Observer Design

On the basis of the Luenberger observer theory [20], the observer (6) can be proposed for system (3) and (4):

$$\begin{cases} \dot{\hat{\dot{\psi}}} = a_{11}\hat{\dot{\psi}} + a_{12}\hat{\beta} + b_1\delta + L_1\tilde{\dot{\psi}} \\ \dot{\hat{\beta}} = a_{21}\hat{\dot{\psi}} + a_{22}\hat{\beta} + b_2\delta + L_2\tilde{\dot{\psi}}, \end{cases} \tag{6}$$

where $\hat{X} = (\hat{\dot{\psi}} \quad \hat{\beta})^{\mathrm{T}}$ is the observer output, $L = (L_1 \quad L_2)^{\mathrm{T}}$ is the observer gain matrix and $\tilde{\dot{\psi}}$ is the yaw rate observation error.

It leads to the following two observation error equations:

$$\begin{cases} \dot{\widetilde{\dot{\psi}}} = (a_{11} - L_1)\widetilde{\dot{\psi}} + a_{12}\widetilde{\beta} \\ \dot{\widetilde{\beta}} = (a_{21} - L_2)\widetilde{\dot{\psi}} + a_{22}\widetilde{\beta}. \end{cases} \tag{7}$$

The stability of the observer can be demonstrated by considering the Lyapunov function candidate $V_1(\widetilde{X}) = \frac{1}{2}(\widetilde{\dot{\psi}}^2 + \widetilde{\beta}^2)$. Relying on (7), the time derivative of V_1 is:

$$\dot{V}_1 = ((a_{11} - L_1)\widetilde{\dot{\psi}} + a_{12}\widetilde{\beta})\widetilde{\dot{\psi}} + ((a_{21} - L_2)\widetilde{\dot{\psi}} + a_{22}\widetilde{\beta})\widetilde{\beta}. \tag{8}$$

Then, if the observer gain L_2 is set to $L_2 = a_{12} + a_{21}$, the time derivative of V_1 can be written as:

$$\dot{V}_1 = (a_{11} - L_1)\widetilde{\dot{\psi}}^2 + a_{22}\widetilde{\beta}^2. \tag{9}$$

According to their definition, the two coefficients a_{11} and a_{22} are strictly negative (since C_f and C_r are strictly positive). As a consequence, if the observer gain L_1 is strictly positive, the time derivative of V_1 is strictly negative. This ensures the asymptotic stability of the observer state.

Moreover, the choice of a large observer gain L_1 ensures observer robustness even when L_2 is slightly different from its expected value equal to $a_{12} + a_{21}$ (which is always the case in practice).

3.2. Simulated Results

A bicycle model was simulated using MATLAB software. This simulator was based on the model shown in Fig. 1 and includes a Pacejka tire/ground model [18] with parameters consistent with manoeuvres on a low grip terrain (this corresponds to model (1), where $C_\text{f}(\cdot)$ and $C_\text{r}(\cdot)$ are obtained from the magic formula). Here, the off-road vehicle considered is a quad bike. Its main parameters, used for the simulations, are listed in Table 1.

The LO has been developed considering that the tire stiffnesses are known and have a constant value. A simulation test was performed to investigate how inaccurate the LO is when these assumptions are no longer satisfied. During this simulation, sharp changes are imposed on the velocity and the steering angle, as shown in Fig. 2. The steady-state values for these two variables are respectively 36 km/h and 12° so that, in view of the ground contact parameters, the tire/ground lateral forces enter the non-linear area at time $t = 1.5$ s.

Table 1.
Quad bike parameters used in simulation

Yaw momentum of inertia I_z	130 kgm^2
Half-front wheelbase a	0.6 m
Half-rear wheelbase b	0.7 m
Quad bike weight m	250 kg

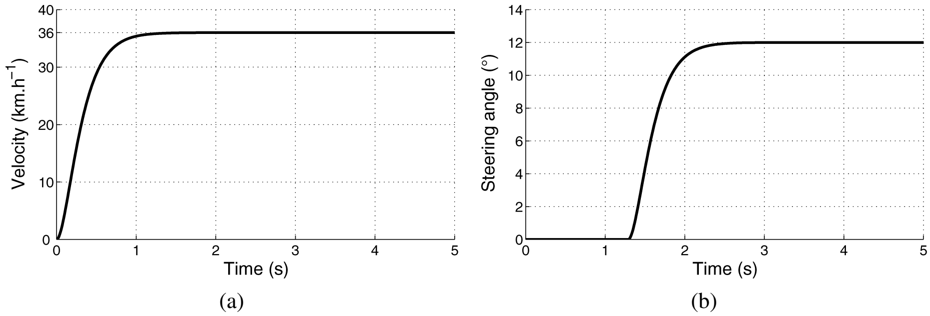

Figure 2. (a) Velocity and (b) steering angle imposed.

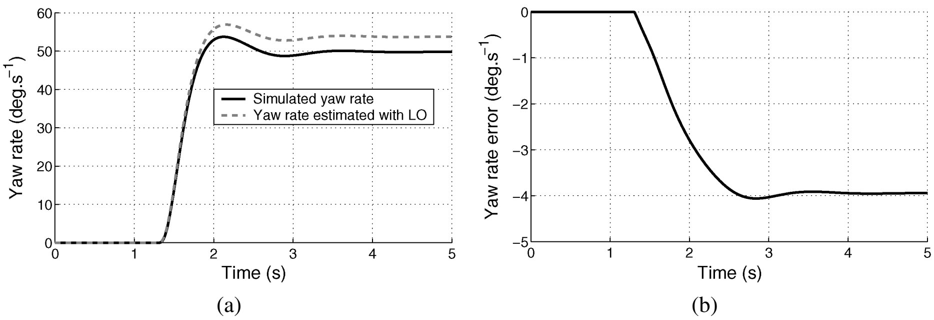

Figure 3. LO results. (a) Yaw rate estimation with LO. (b) Yaw rate estimation error with LO.

The Fig. 3 shows the estimated yaw rate and the yaw rate error supplied by the linear observer when $L_2 = a_{12} + a_{21}$ and $L_1 = 100$.

As expected, the yaw rate is no longer satisfactorily estimated when tire/ground contact non-linearity is encountered at time $t = 1.5$ s (see Section 3.4.1). Therefore, in such situations, the future yaw rate cannot be accurately predicted and a rollover risk indicator based on such a variable would be erroneous, as pointed out in Ref. [10].

As a consequence, tire cornering stiffness non-linearity and variability have to be taken into account. One solution could consist in using both a tire stiffness adaptation law and the linear observer. This would require the measurement of both the yaw rate and the global sideslip angle of the vehicle. Unfortunately, the latter is not available with our sensor configuration (and is hard to obtain with other sensors as well). Consequently, an adapted backstepping observer is proposed below to estimate on-line a tire cornering stiffness representative of the non-linear tire/ground contact behavior.

3.3. Adapted Backstepping Observer (ABO)

3.3.1. Principle

When tire cornering stiffness is considered as constant (noted C_0 in Fig. 4), the linear tire/ground contact model (1) is only able to describe the pseudo-sliding area of

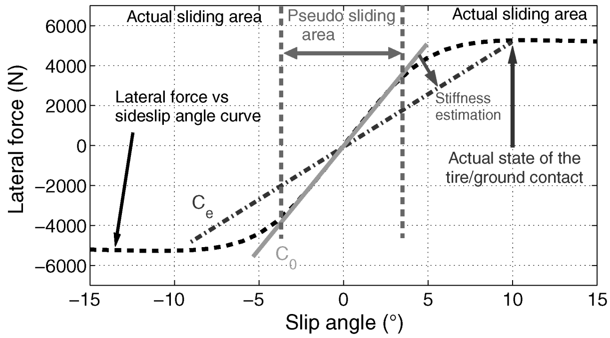

Figure 4. Estimation principle of the tire cornering stiffness.

the tire. However, since ATVs are expected to move on slippery ground, tire/ground forces are highly non-linear. The approach proposed in this paper to satisfactorily estimate lateral forces, even in the non-linear area, consists in updating a virtual tire cornering stiffness C_e, as shown in Fig. 4, so as to reflect variations in grip conditions. Model (1) could, therefore, reflect both a pseudo-sliding area ($C_e = C_0$) and actual sliding ($C_e < C_0$, see blue dashed line in Fig. 4).

As mentioned above, only three measurements are available from our sensor configuration: the yaw rate $\dot{\psi}$, the steering angle δ and the rear axle linear velocity v. As a consequence, C_f and C_r cannot be estimated separately, and are considered to be equal to a virtual tire cornering stiffness C_e. In view of (5), the system is still observable if $a \neq b$ and of course if $v \neq 0$, conditions ensured in practice.

3.3.2. Backstepping Design

The main idea is to design the observation algorithm using a backstepping approach. Let us write the observer equations as follows:

$$\begin{cases} \ddot{\widehat{\psi}} = a_{11}\dot{\widehat{\psi}} + a_{12}\widehat{\beta} + b_1\delta \\ \dot{\widehat{\beta}} = a_{21}\dot{\widehat{\psi}} + a_{22}\widehat{\beta} + b_2\delta. \end{cases} \tag{10}$$

The first step in the observation algorithm consists in ensuring the convergence of the yaw rate observer error ($\dot{\tilde{\psi}} = \dot{\psi} - \dot{\widehat{\psi}}$) to zero by treating $\widehat{\beta}$ as a control input.

If the following observer dynamics is chosen:

$$\ddot{\tilde{\psi}} = K\dot{\tilde{\psi}}, \quad K < 0, \tag{11}$$

then:

$$\ddot{\widehat{\psi}} = \ddot{\psi} - \ddot{\tilde{\psi}} = \ddot{\psi} - K\dot{\tilde{\psi}} = a_{11}\dot{\widehat{\psi}} + a_{12}\widehat{\beta} + b_1\delta. \tag{12}$$

The control law expression $\overline{\beta}$ for the intermediate control variable $\widehat{\beta}$ can then easily be obtained:

$$\overline{\beta} = \frac{\ddot{\psi} - K\dot{\tilde{\psi}} - a_{11}\dot{\widehat{\psi}} - b_1\delta}{a_{12}}, \tag{13}$$

with $a_{12} \neq 0$ (which is ensured using the assumption mentioned above) and where $\ddot{\psi}$ is the filtered numerical derivative of the measured yaw rate $\dot{\psi}$ (as can be seen in Section 3.4, the delay introduced by the filter is not significant).

With such a choice, the dynamics of the observed yaw rate is now provided by:

$$\ddot{\widehat{\psi}} = a_{11}\dot{\widehat{\psi}} + a_{12}\overline{\beta} + b_1\delta. \tag{14}$$

Since $\overline{\beta}$ ensures that $\dot{\widehat{\psi}}$ converges with the actual value $\dot{\psi}$ supplied by the gyrometer, the virtual control $\overline{\beta}$ appears as a virtual measurement of the global sideslip angle β, to be reached by $\widehat{\beta}$. The second step therefore consists in achieving this convergence by adapting the global tire cornering stiffness C_e. If the following dynamics is chosen:

$$\dot{\widetilde{\beta}} = G\widetilde{\beta}, \quad G < 0, \tag{15}$$

with $\widetilde{\beta} = \overline{\beta} - \widehat{\beta}$ and $|G| \ll |K|$ in such a way that $|\dot{\widetilde{\psi}}|$ decreases faster than $|\widetilde{\beta}|$, then:

$$\dot{\widetilde{\beta}} = \dot{\overline{\beta}} - a_{21}\dot{\widehat{\psi}} - a_{22}\widehat{\beta} - b_2\delta = G\widetilde{\beta}, \tag{16}$$

where $\dot{\overline{\beta}}$ is the filtered numerical derivative of $\overline{\beta}$.

By expanding the a_{ij} coefficients according to (3), the following expression for C_e can be obtained from (16):

$$C_\mathrm{e} = \frac{\dot{\overline{\beta}} + \dot{\widehat{\psi}} - G\widetilde{\beta}}{f(\dot{\widehat{\psi}}, \widehat{\beta}, \delta)}, \tag{17}$$

where $f(\dot{\widehat{\psi}}, \widehat{\beta}, \delta)$ is given by:

$$f(\dot{\widehat{\psi}}, \widehat{\beta}, \delta) = \frac{(b-a)\dot{\widehat{\psi}}}{mv^2} - \frac{2\widehat{\beta}}{mv} + \frac{\delta}{mv}. \tag{18}$$

In view of (18), the estimation of the global tire cornering stiffness is properly defined as soon as $v \neq 0$ and $\delta \neq 0$. Indeed, if $\delta = 0$ (straight line), $\widehat{\beta}$ and $\dot{\widehat{\psi}}$ also converge to zero, so that (17) is undefined and C_e cannot be estimated. Since this last singularity is likely to occur, the rule was imposed that close to neutral steering, virtual cornering stiffness is not adapted but holds to its previous value.

3.4. Simulated Results

In this section, two sets of simulations are reported. The first one is similar to that presented in Section 3.2 and relies on MATLAB. The second one was performed using the multibody simulation software Adams, in order to simulate actual conditions more realistically.

3.4.1. MATLAB Simulation

In order to compare the ABO with the LO, the same velocity and steering angle inputs as those shown in Fig. 2 were used. The yaw rate estimation achieved by the backstepping observer is reported in Fig. 5.

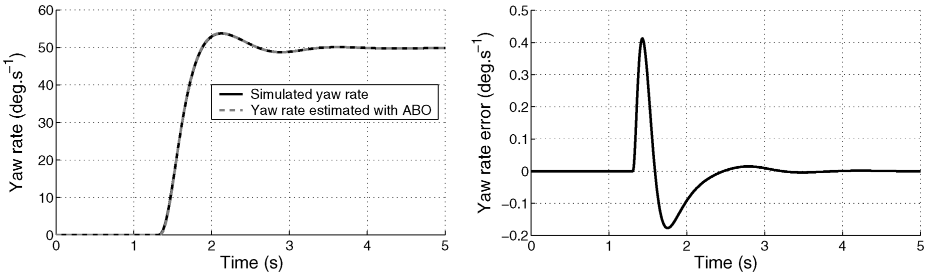

(a) (b)

Figure 5. ABO results. (a) Yaw rate estimation with ABO. (b) Yaw rate estimation error $\tilde{\dot{\psi}}$ with ABO.

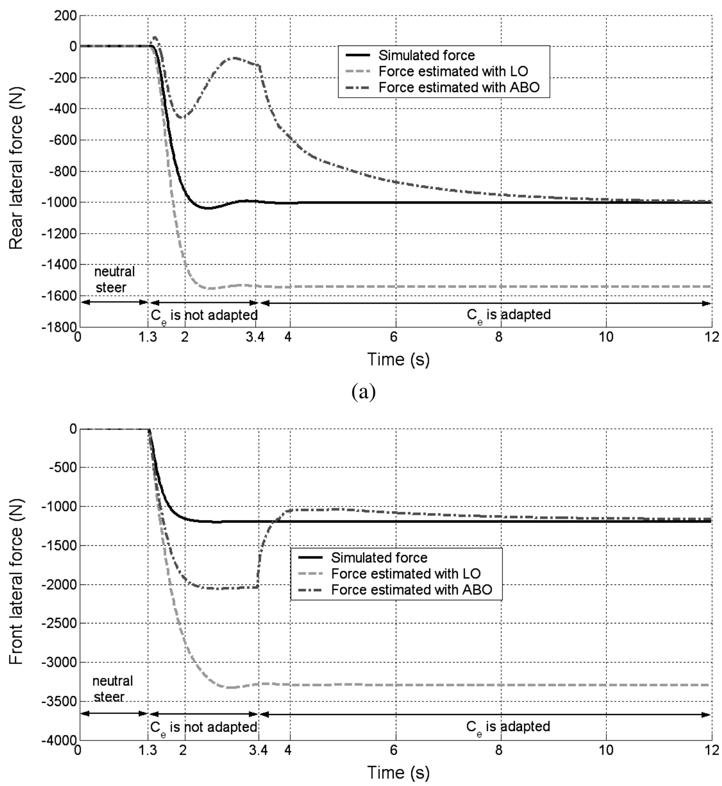

(b)

Figure 6. (a) Rear and (b) front lateral forces estimation results.

Contrary to Fig. 3, it can be observed in Fig. 5 that the yaw rate estimated with the ABO is satisfactorily superposed with the simulated one. Thus, on the basis of the adapted cornering stiffness (17), and the rear and front sideslip angles estimated from (2), the rear and front lateral forces can be computed. In Fig. 6, the lateral forces estimated by ABO with an initial value of $C_{\mathrm{e}} = 20\,000$ N/rad and by LO (when the cornering stiffness is equal to the pseudo-sliding one $C_0 = 20\,000$ N/rad)

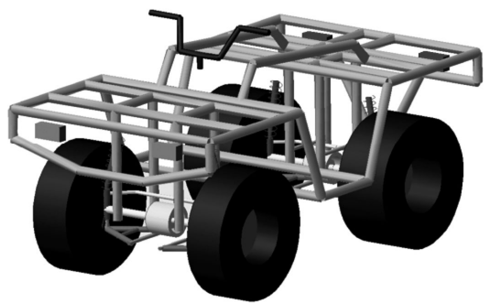

(a)

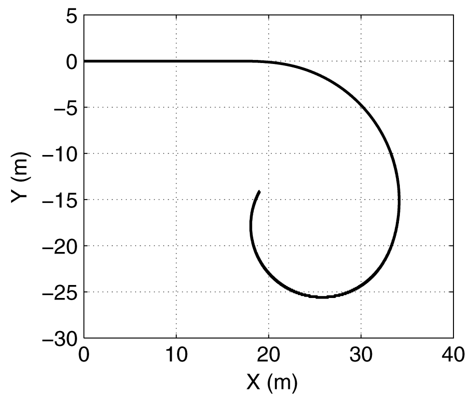

(b)

Figure 7. (a) Virtual quad bike and (b) path followed.

are both compared to the simulated ones. It can be observed that the lateral forces provided by ABO converge with the measured values as soon as C_e begins to be adapted, as shown in Fig. 6 (before $t = 1.3$ s, no observation is performed, since the vehicle is in a neutral steer situation, then between $t = 1.3$ s and $t = 3.4$ s C_e is not adapted, and, finally, C_e begins to be adapted at $t = 3.4$ s). Therefore, when non-linear sliding occurs, only lateral forces estimated with ABO are able to reflect the simulated forces. In contrast, the lateral forces computed with the LO are greatly overestimated. This demonstrates the capabilities of the proposed observer.

3.4.2. Adams Simulation Results

A virtual quad bike, shown in Fig. 7a, was built using the parameters listed in Table 1. The low grip conditions were set using the Adams contact properties. This software is able to achieve realistic simulations closely resembling disturbances encountered in actual experiments. In Adams, all the body geometry, joints and external forces are entered without specifying explicit mechanical equations. The vehicle's motion is then numerically computed and can be considered as a virtual test bed to demonstrate the robustness of our algorithms previously investigated in the ideal case with MATLAB.

The rear axle velocity, yaw rate and steering angle were recorded by Adams with a frequency of 100 Hz (identical to that of the gyrometer). The path followed by the vehicle consists of a straight line, enabling the vehicle to reach a 21 km/h constant velocity. Two curves were then performed, with a steering angle value equal to 5° for the first and to 10° for the second.

In Fig. 8, we can check the accuracy of the ABO for the estimation of the yaw rate simulated on Adams: during each bend (between $t = 8$–13 s and $t = 13$–18 s) the yaw rate observation error converges to zero. In order to satisfactorily estimate this variable, global tire stiffness is adapted, as reported in Fig. 8b. Several simulations with different initial values for tire stiffness have been achieved: $C_{\text{init1}} = 5\,000$ N/rad, $C_{\text{init2}} = 50\,000$ N/rad and $C_{\text{init3}} = 100\,000$ N/rad. It is notice-

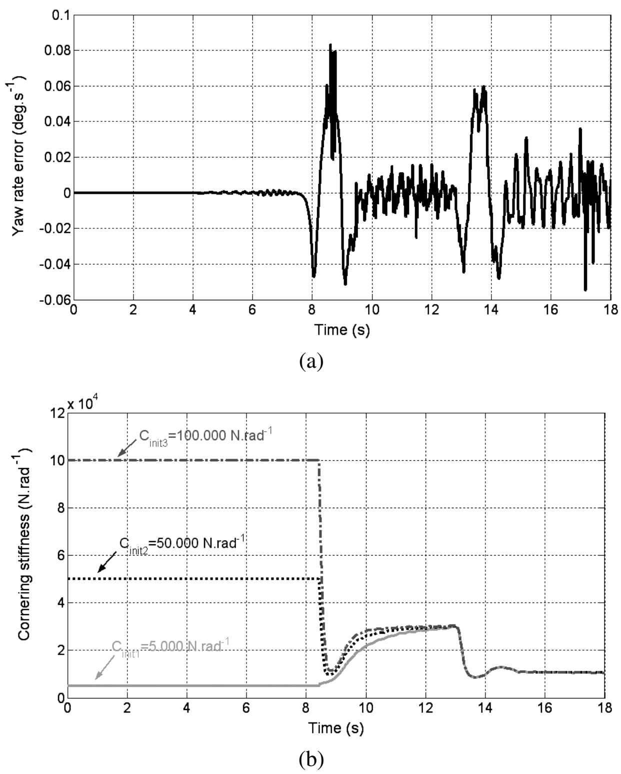

Figure 8. Advanced simulation results. (a) Yaw rate estimation error. (b) Adapted cornering stiffness.

able that the initial value has no impact on the estimated tire cornering stiffness supplied by the algorithm after the transient phase — the three curves are superposed after $t = 12$ s. In Fig. 8b, it can also be seen that during the straight line, C_e is not adapted consistently with comments relating to (17).

Finally, in Fig. 9, the lateral forces measured with Adams were compared between $t = 8$ s and $t = 18$ s with those estimated by ABO and LO, when the initial tire stiffness value being set to 50 000 N/rad.

First, it can be observed that during the first curve, since the sliding phenomenon is not very significant, the estimations of the lateral forces computed either from LO or ABO are both accurate.

During the second curve ($t = 13$–18 s), where sliding is increased, the lateral forces computed from LO (assuming a constant tire cornering stiffness) are no longer relevant. In contrast, due to the tire cornering stiffness adaptation, the lateral forces computed from ABO stay close to those measured. The estimated value of global tire cornering stiffness, supplied by ABO, is then meaningful for prediction of the yaw rate and can then reliably be used to compute the lateral load transfer of the vehicle.

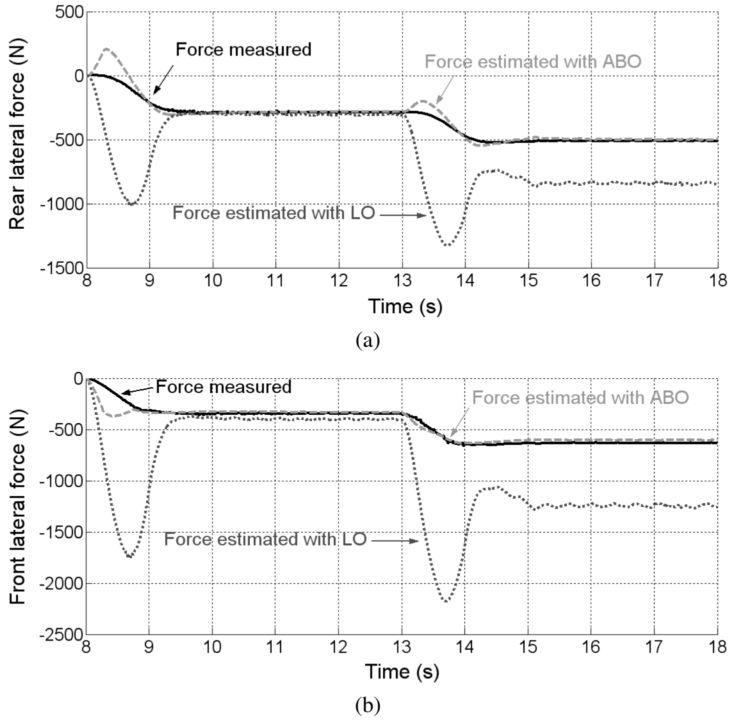

Figure 9. Lateral forces estimation results. (a) Rear lateral force. (b) Front lateral force.

4. Application to LLT Computation

In this section, we show how the adapted backstepping observer was used to compute the LLT:

$$\mathrm{LLT} = \frac{F_{n1} - F_{n2}}{F_{n1} + F_{n2}}, \tag{19}$$

where F_{n1} and F_{n2} are the normal forces on the vehicle's left and right sides (as shown in Fig. 10). These two forces are derived from a vehicle roll model (see Ref. [10]) and rely on the vehicle's lateral acceleration. As a result, a relevant LLT computation in a natural environment requires tire stiffness, sideslip angles and yaw rate estimation as performed by our adapted observer.

Clearly, a rollover situation is detected when a unitary value of |LLT| is reached, since it corresponds to the lift-off of the wheels on the same side of the vehicle. Here, the vehicle's behavior will be considered as hazardous when LLT reaches the critical threshold 0.8. On flat ground, the LLT computation algorithm inputs are the vehicle's velocity, the steering angle, the yaw rate and the global sideslip angle obtained from the adapted cornering stiffness (17).

Advanced simulation results are first presented in order to show the theoretical validity of the approach. Then, experimental results performed on a Kymco Mxer

150 quad bike shown in Fig. 10 demonstrate the capability of the method through full-scale tests.

4.1. Advanced Simulation Results

The virtual quad bike shown in Fig. 7a was used to perform a simulation where the vehicle steering angle and velocity were, respectively, equal to 15° and 23 km/h. The grip conditions imposed correspond to driving on wet grass. The changes in LLT over time measured with Adams are shown in a black solid line in Fig. 11 and are compared to the LLT computed from the three measurements recorded in Adams (yaw rate, rear axle linear velocity and steering angle) with a constant cornering stiffness $C_0 = 40\,000$ N/rad (high grip ground, top dashed line), $C_0 = 2000$ N/rad (very slippery ground, bottom dashed line) and with the adapted cornering stiffness C_e when its initial value is 40 000 N/rad (middle dashed line). Furthermore, the changes in adapted cornering stiffness are shown in Fig. 12 with initial values respectively equal to $C_{init1} = 10\,000$ N/rad, $C_{init2} = 20\,000$ N/rad and

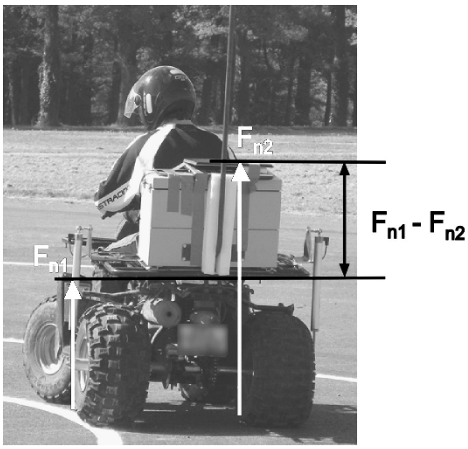

Figure 10. Vehicle normal forces during a turn to the left.

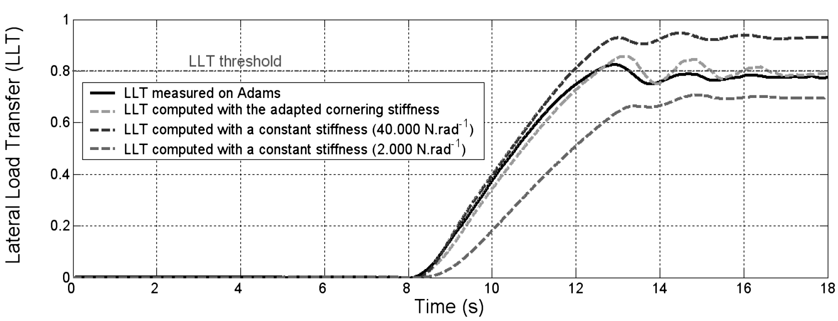

Figure 11. Lateral load transfer comparison on advanced simulation.

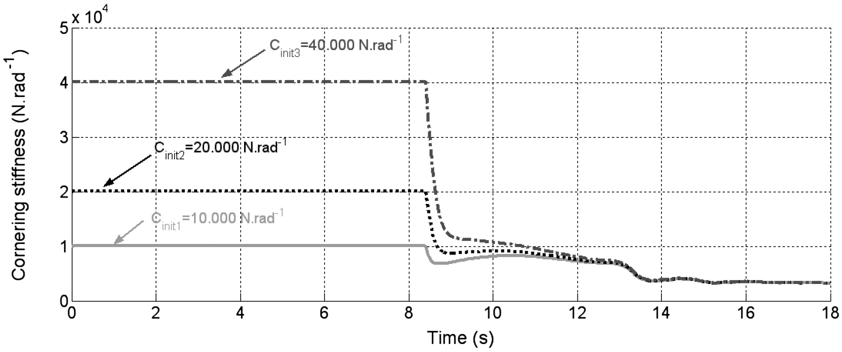

Figure 12. Adapted cornering stiffness C_e.

$C_{init3} = 40\,000$ N/rad. As explained in Section 3.4.2, it can be observed that the initial value has no impact on the adapted cornering stiffness.

With constant stiffness $C_0 = 40\,000$ N/rad, LLT is greatly overestimated and stabilizes below the rollover threshold 0.8. At time $t = 18$ s, it presents a 15% error with respect to the LLT provided by Adams.

In contrast, with the constant stiffness $C_0 = 2000$ N/rad, LLT is greatly underestimated and the potentially hazardous situation cannot be detected. The maximum error with respect to the LLT supplied by Adams is equal to 30%.

Finally, the LLT computed with the adapted C_e does not provide any erroneous information: the maximum error with respect to the LLT supplied by Adams does not exceed 4% and, after a transient period (e.g., at $t = 18$ s), the error is negligible. This demonstrates the relevancy of the backstepping observer to accurate computing of LLT values when sliding occurs. Moreover, when the design parameters (mass, lengths, etc.) are badly identified, adapted cornering stiffness is less representative of actual grip conditions (lateral forces are inaccurate) but will still ensure the convergence of $\tilde{\dot{\psi}}$ to zero. Consequently, as the yaw rate is the dominant variable of the vehicle's lateral acceleration (see Ref. [21]), the accuracy of the LLT is conserved, since the normal forces are still accurate.

4.2. Actual Experimental Results

The parameters of the Kymco Mxer 150 quad bike with driver, shown in Fig. 13a, are listed in Table 2.

In order to compare the computed LLT with reality on the ground, the quad bike was equipped with four linear potentiometers fixed parallel to the suspensions. After a preliminary calibration, these enable measurement of the actual LLT. Nevertheless this reality on the ground is expensive and difficult to implement, and therefore could not be used in commercial applications.

The experiments were conducted on flat ground mainly constituted of dry grass. The path followed is shown in Fig. 13b and consists of straight lines and half turns. The quad bike speed was between 15 and 25 km/h.

(a)

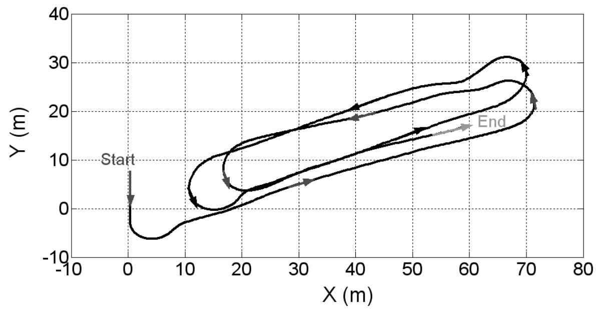

(b)

Figure 13. Actual experiments. (a) Kymco Mxer 150. (b) Path followed during experiments.

Table 2.
Kymco Mxer 150 parameters

Quad bike mass with sensors	220 kg
Driver mass with equipment	90 kg
I_x, I_y, I_z	57, 105, 83 kgm^2
Front and rear half-wheelbases a, b	0.66, 0.48 m
Quad bike track c	0.67 m

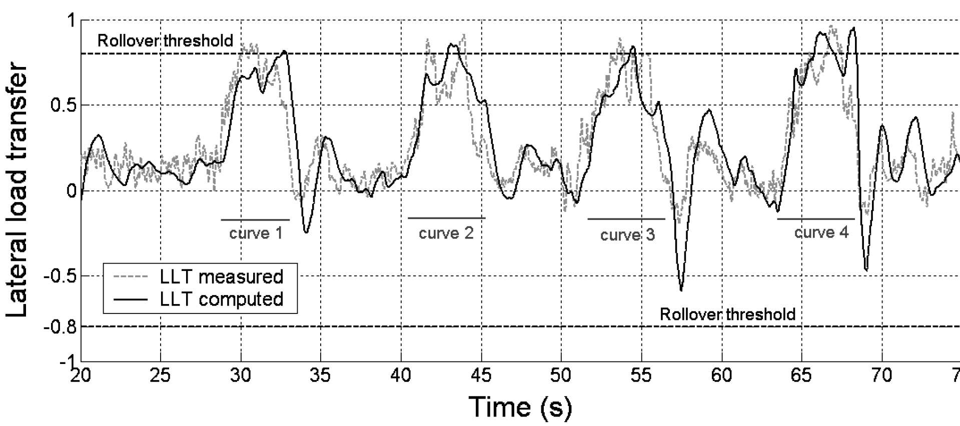

Figure 14. LLT comparison.

Relying on the measured velocity, steering angle and yaw rate, tire cornering stiffness was estimated, and the lateral load transfer was then computed and compared to that measured in Fig. 14.

When observing the four half turns, it can be observed that the computed LLT is satisfactorily superposed on the measured value. In each curve, the measured LLT crosses the threshold value 0.8, and so does the computed LLT. This demonstrates the ability of the computed LLT to detect hazardous situations.

Finally, some negative overshoots at the end of each curve can be observed on the computed LLT. They correspond to an actual dynamics (as can be seen in the video of the experiment) that cannot be measured by the normal force measurement system. The linear potentiometers are indeed attached to the suspensions, which cannot reach total expansion instantaneously. As a consequence, the length supplied by the potentiometer is also damped and the measured LLT is barely equal to 1.

5. Conclusions and Future Work

5.1. Conclusions

This paper proposes an ABO to estimate global tire cornering stiffness from yaw rate observation. It is expected to be used to supply on-line relevant values to a rollover risk indicator dedicated to off-road vehicles. A dynamic bicycle model, as well as a tire/ground description, have been detailed. Based on these representations, a preliminary linear yaw rate observer (LO) was developed on the assumption that tire cornering stiffness is constant. It was then shown that the observed yaw rate error no longer converges to zero as soon as tire/ground forces enter the non-linear zone. This indicates the necessity of adapting tire cornering stiffness on-line for accurate prediction of the vehicle's behavior in such situations. This is the aim of the backstepping observer proposed in this paper (ABO). It was designed in to two steps. In the first one, the yaw rate was estimated from a virtual measurement of global sideslip angle. In the second step, global tire cornering stiffness was adapted in order to ensure the convergence of the global sideslip angle value to this virtual measurement. The relevance of this approach was then investigated through both advanced simulations and the computation of the LLT in full-scale experiments. Both of these tests demonstrate the applicability and relevancy of the proposed approach.

5.2. Future Work

The extension of the proposed work to additional sensors is currently under investigation and could enable improved estimation of global sideslip angle and consequently the estimation of global tire cornering stiffness.

Finally, on-line adaptation of tire cornering stiffness offers a relevant input to address ATV stability. Our research work is mainly concerned with developing on-board devices for ATV rollover avoidance. Such systems are intended to be designed on the basis of constrained and optimal control approaches.

References

1. US Consumer Product Safety Commission, 2005 annual report of ATV deaths and injuries, *Technical report*, CPSC, Washington, DC (2006).
2. CCMSA, Accidents du travail des salariés et non salariés agricoles avec des quads, *Technical Report*, Observatoire des Risques Professionels et du Machinisme Agricole, Paris (2006).
3. B. Schofield, Vehicle dynamics control and controller allocation for rollover prevention, in: *Proc. 15th IEEE Conf. on Control Applications*, Munich, pp. 149–154 (2006).

4. J. Ackermann, D. Odenthal and T. Bünte, Advantages of active steering for vehicle dynamics control, in: *Proc. Int. Conf. on Advances in Vehicle Control and Safety*, Amiens, 112–117 (1998).
5. R. Bosch, *Safety, Comfort and Convenience Systems*. Wiley, Hoboken (2006).
6. National Highway Traffic Safety Administration, Trends in static stability factor of passengers cars, light trucks and vans, *Technical Report*, Department of Transportation, Washington, DC (2005).
7. R. Whitehead, W. Travis, D. M. Bevly and G. Flowers, A study of the effect of various vehicle properties on rollover propensity, *SAE Int.* (2004-01-2094) 2004.
8. P. Sardain and G. Bessonet, Forces acting on a biped robot. Center of pressure — zero moment point, *IEEE Trans. Syst. Man Cybernet.* **34**, 630–637 (2004).
9. M. Vukobratovic, On the stability of anthropomorphic systems, *Math. Biosci.* **15**, 1–37 (1972).
10. N. Bouton, R. Lenain, B. Thuilot and J.-C. Fauroux, A rollover indicator based on the prediction of the load transfer in presence of sliding: application to an all terrain vehicle, in: *Proc. Int. Conf. on Robotics and Automation*, Rome, pp. 1158–1163 (2007).
11. N. Bouton, R. Lenain, J.-C. Fauroux and B. Thuilot, Dynamic modelling of all-terrain vehicles designed for dynamic stability analysis, in: *Proc. Conf. on Multibody Dynamics*, Milan (2007).
12. J. Ryu and J. C. Berges, Vehicle sideslip and roll parameter estimation using GPS, in: *Proc. 6th Int. Symp. on Advanced Vehicle Control*, Hiroshima (2002).
13. R. Anderson and D. M. Bevly, Estimation of slip angles using a model based estimator and GPS, in: *Proc. Am. Control Conf.*, Boston, MA, pp. 2122–2127 (2004).
14. R. Anderson and D. M. Bevly, Estimation of tire cornering stiffness using GPS to improve model based estimation of vehicle states, in: *Proc. IEEE Intelligent Vehicles Conf. IV*, Las Vegas, NV, pp. 801–806 (2005).
15. C. Canudas de Wit, B. Siciliano and G. Bastin, *Theory of Robot Control*. Springer, Berlin (1996).
16. R. Lenain, B. Thuilot, C. Cariou and P. Martinet, High accuracy path tracking for vehicles in presence of sliding: application to farm vehicle automatic guidance for agricultural tasks, *Autonomous Robots* **21**, 79–97 (2006).
17. J. Stephant, A. Charara and D. Meizel, Force model comparison on the wheel-ground contact for vehicle dynamics, in: *Proc. IEEE Intelligent Vehicle Symp.*, Versailles, pp. 589–593 (2002).
18. H. B. Pacejka, E. Bakker and L. Nyborg, Tyre modelling for use in vehicle dynamics studies, *SAE Paper* (870421) (1987).
19. R. Lenain, Contribution à la modélisation et à la commande de robots mobiles en présence de glissement, *PhD Thesis*, Université Blaise Pascal, Clermont-Ferrand (2005).
20. T. Meurer, K. Graichen and E. D. Gilles, *Control and Observer Design for Nonlinear Finite and Infinite Dimensional Systems*. Springer, Berlin (2005).
21. D. Odenthal, T. Bünte and J. Ackermann, Nonlinear steering and braking control for vehicle rollover avoidance, in: *Proc. Eur. Control Conf.*, Karlsruhe (1999).

About the Authors

Nicolas Bouton has been a PhD student in Cemagref on the topic of Agriculture Robotics and Safety since 2006. He graduated from the French Institute for Advanced Mechanics, Clermont-Ferrand, France, and received his Master title in Robotics from Blaise Pascal University of Clermont-Ferrand, France, in 2006. His research interests include the development of automatic devices for farmer comfort, environmental aspects and safety.

Roland Lenain is a Research Fellow in Cemagref on the topic of Agricultural Robotics. His research interests include the modeling and the control of agricultural vehicles. The aims of research are the development of automatic devices for farmer comfort, environmental aspects and safety. He graduated from the French Institute for Advanced Mechanics, in 2002. He received his PhD degree in Robotics from Blaise Pascal University, in 2005. He held a Postdoctoral appointment at Lund University, Sweden, in 2006.

Benoit Thuilot received his Electrical Engineering and PhD degrees in 1991 and 1995. He held a Postdoctoral appointment at the INRIA research units of Grenoble, France, in 1996, and Sophia-Antipolis, France, in 1997. Since 1997, he has been an Assistant Professor at Blaise Pascal University of Clermont-Ferrand, France. He is also a Research Scientist at LASMEA-CNRS Laboratory, Clermont-Ferrand, France. His research interests include non-linear control of mechanical systems, with application to automatic guided vehicles. Intelligent transportation systems and off-road vehicles are both addressed.

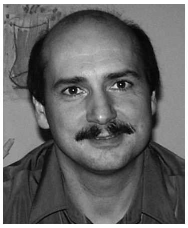

Philippe Martinet graduated from the CUST, Clermont-Ferrand, France, in 1985, and received the PhD degree in Electronics Science from Blaise Pascal University, Clermont-Ferrand, France, in 1987. Since 2000, he has been a Professor with the French Institute for Advanced Mechanics, Clermont-Ferrand. He conducts research at the Robotics and Vision Group of LASMEA-CNRS, Clermont-Ferrand. He is the Leader of the group. His research interests include visual servoing, vision-based control, robust control, automatic guided vehicles, enhanced mobility, active vision and sensor integration, visual tracking, and parallel architecture for visual servoing.